

# 1 Deep Dive into Hydrologic Simulations at Global Scale: Harnessing the Power of Deep 2 Learning and Physics-informed Differentiable Models ( $\delta$ HBV-globe1.0-hydroDL)

3 Dapeng Feng<sup>1,2,3</sup>, Hylke Beck<sup>4</sup>, Jens de Bruijn<sup>3,5</sup>, Reetik Kumar Sahu<sup>3</sup>, Yusuke Satoh<sup>6</sup>, Yoshihide Wada<sup>7</sup>,  
4 Jiangtao Liu<sup>1</sup>, Ming Pan<sup>8</sup>, Kathryn Lawson<sup>1</sup>, Chaopeng Shen<sup>1\*</sup>

5  
6 <sup>1</sup> Civil and Environmental Engineering, Pennsylvania State University, University Park, PA, USA

7 <sup>2</sup> Earth System Science, Stanford University, Stanford, CA, USA

8 <sup>3</sup> Water Security Research Group, International Institute for Applied Systems Analysis (IIASA), Laxenburg, Austria

9 <sup>4</sup> Climate and Livability Initiative, Physical Science and Engineering Division, King Abdullah University of Science and  
10 Technology, Thuwal, Saudi Arabia

11 <sup>5</sup> Institute for Environmental Studies (IVM), Vrije Universiteit Amsterdam, Amsterdam, Netherlands

12 <sup>6</sup> Moon Soul Graduate School of Future Strategy, Korea Advanced Institute of Science and Technology, Daejeon, Republic of  
13 Korea

14 <sup>7</sup> Climate and Livability Initiative, Center for Desert Agriculture, Biological and Environmental Science and Engineering  
15 Division, King Abdullah University of Science and Technology, Thuwal, Saudi Arabia

16 <sup>8</sup> Center for Western Weather and Water Extremes, Scripps Institution of Oceanography, University of California San Diego,  
17 La Jolla, CA, USA

18 \*Correspondence to: Chaopeng Shen (cshen@engr.psu.edu)

19 **Abstract.** Accurate hydrological modeling is vital to characterizing how the terrestrial water cycle responds to climate change.  
20 Pure deep learning (DL) models have shown to outperform process-based ones while remaining difficult to interpret. More  
21 recently, differentiable, physics-informed machine learning models with a physical backbone can systematically integrate  
22 physical equations and DL, predicting untrained variables and processes with high performance. However, it was unclear if  
23 such models are competitive for global-scale applications with a simple backbone. Therefore, we use - for the first time at this  
24 scale - differentiable hydrologic models (full\_name  $\delta$ HBV-globe1.0-hydroDL, ~~shortened to and shorthanded~~  $\delta$ HBV [here](#)) to  
25 simulate the rainfall-runoff processes for 3753 basins around the world. Moreover, we compare the  $\delta$ HBV models to a purely  
26 data-driven long short-term memory (LSTM) model to examine their strengths and limitations. Both LSTM and the  $\delta$ HBV  
27 models provide competent daily hydrologic simulation capabilities in global basins, with median Kling-Gupta efficiency  
28 values close to or higher than 0.7 (and 0.78 with LSTM for a subset of 1675 basins with long-term records), significantly  
29 outperforming traditional models. Moreover, regionalized differentiable models demonstrated stronger spatial generalization  
30 ability (median KGE 0.64) than a traditional parameter regionalization approach (median KGE 0.46) and even LSTM for  
31 ungauged region tests in Europe and South America. Nevertheless, relative to LSTM, the differentiable model was hampered  
32 by structural deficiencies for cold or polar regions, and highly arid regions, and basins with significant human impacts. This

33 study also sets the benchmark for hydrologic estimates around the world and builds foundations for improving global  
34 hydrologic simulations.

35

36 **Short Summary.** Accurate hydrological modeling is vital to characterizing water cycle responses to climate change. For the  
37 first time at this scale, we use differentiable physics-informed machine learning hydrologic models to simulate rainfall-runoff  
38 processes for 3753 basins around the world and compare them with purely data-driven and traditional approaches. This sets a  
39 benchmark for hydrologic estimates around the world and builds foundations for improving global hydrologic simulations.

40

41 **Key Words.** Physics-informed machine learning; Differentiable hydrologic models; Global hydrologic modeling; high  
42 resolution evaluation; Parameter regionalization; Prediction in ungauged regions

## 43 1. Introduction

44 Hydrological models are vital tools to model and elucidate the terrestrial water cycle, and have been widely used in flood  
45 forecasting (Maidment, 2017), water resources management (Jayakrishnan et al., 2005), and assessing climate change impacts  
46 (Hagemann et al., 2013). Recently, deep learning (DL) models have demonstrated superior performance compared to  
47 traditional process-based hydrological models in accurately predicting different components of the hydrologic cycle (Shen,  
48 2018), such as soil moisture (Fang et al., 2017, 2019; Fang and Shen, 2020), streamflow (Feng et al., 2020; Konapala et al.,  
49 2020; Kratzert et al., 2019b; [Liu et al. 2024](#)), [snow water equivalent \(Cui et al., 2023; Song et al., 2024\)](#), groundwater (Wunsch  
50 et al., 2021) and water quality (Hansen et al., 2022; Rahmani et al., 2021; Saha et al., 2023; Zhi et al., 2021; [Chaemchuen et  
51 al., 2023](#)). Long short-term memory (LSTM) networks, which are a type of recurrent neural network (Hochreiter and  
52 Schmidhuber, 1997), [and Transformers](#) are currently popular DL algorithms for handling time series dynamics in hydrology,  
53 while other architectures like transformers can also be employed. LSTM models have established state-of-the-art accuracy for  
54 streamflow prediction at continental and smaller scales (Feng et al., 2020, 2021; Kratzert et al., 2019a, b; Lees et al., 2021;  
55 Mai et al., 2022).

56

57 Although DL models have shown great prediction accuracy compared to traditional models, they usually do not possess clear  
58 physical constraints inside the model and are often considered to be “black boxes”, despite recent efforts shed by some  
59 interpretive efforts (Lees et al., 2022). Thus, purely data-driven models are limited in that they cannot predict unobservable or  
60 untrained physical variables, [and ~~Therefore, a data-driven DL model impedes~~](#) the investigation of the physical relations of  
61 different hydrologic variables behind the change in the target variable. [They may also become overfitted and acquire incorrect  
62 sensitivities to inputs \(Reichert et al., 2024\)](#). In contrast, traditional process-based hydrologic models following physical laws  
63 like mass balances can provide a full set of diagnostic outputs for hydrologic variables like soil water storage, groundwater  
64 recharge, evapotranspiration and snow water equivalent, even though they are usually only calibrated on discharge

65 observations (Burek et al., 2020; Müller Schmied et al., 2014). The multivariate output nature of these models provides an  
66 opportunity for calibration on one or more observable variables to better predict other, perhaps unobservable, variables (in  
67 reality, whether this is the case or not depends on if the issue of parameter non-uniqueness is addressed). However, it seems  
68 quite difficult for the traditional physical model to approach the performance level of the DL models in daily hydrograph  
69 metrics (Feng et al., 2020; Kratzert et al., 2019b) or to improve in generalization with increasing training data (Tsai et al.,  
70 2021). In addition, traditional calibration is typically done site-by-site and can be time- and labor-intensive. Therefore, it  
71 logically follows that integrating DL and process-based models might enable harnessing their respective strengths while  
72 circumventing their weaknesses (Shen et al., 2023).

73

74 By combining a physical model with a DL model, differentiable modeling (Shen et al., 2023) provides a systematic solution  
75 to leveraging the strengths of both model types while circumventing their limitations. In differentiable models, we use process-  
76 based models as a backbone and insert neural networks to either provide parameters (Tsai et al., 2021) or process substitutes  
77 for physical models (Aboelyazeed et al., 2023; Feng et al., 2022, 2023; Höge et al., 2022; Jiang et al., 2020), or they could use  
78 limited physical constraints (Kraft et al., 2022). They are collectively called “differentiable models” in the sense that they can  
79 rapidly compute gradients of outputs with respect to inputs or parameters using automatic differentiation (or any other means).  
80 The differentiability enables the training of neural network components placed anywhere in the model via backpropagation.  
81 Inserting neural networks into process-based models can be perceived as posing questions regarding some uncertain  
82 relationships given some known ones (priors) and we want to get answers for these questions by automatically learning from  
83 big data.

84

85 Some of our recent work has applied differentiable modeling to the conceptual hydrologic model named Hydrologiska Byråns  
86 Vattenbalansavdelning (HBV) (Bergström, 1976, 1992; Seibert and Vis, 2012), and built a physics-informed hybrid model for  
87 basins in the contiguous United States (CONUS) (Feng et al., 2022, 2023). The model is “regionalized” in the sense that the  
88 embedded neural network components are trained simultaneously on all basins in the study region in order to provide physical  
89 HBV parameters which are learned from raw information of basin attributes, resulting in improved generalizability and reduced  
90 overfitting to local noise. With the help of differentiable modeling to flexibly evolve the original structure of HBV, the  
91 differentiable hybrid models can approach the performance level of the LSTM model, whilst being constrained to physical  
92 laws and keeping process clarity to predict untrained diagnostic variables with decent accuracy (Feng et al., 2022). Since the  
93 framework is regionalized, this differentiable model can be used to predict in ungauged regions and even extrapolates better  
94 spatially than LSTM in data-sparse regions when tested across the CONUS (Feng et al., 2023).

95

96 Owing to the complexity of calibration, current global hydrologic models are largely either uncalibrated (Hattermann et al.,  
97 2017; Zaherpour et al., 2018) or only calibrated on mean annual water budgets [or](#) in limited regions (Burek et al., 2020; Müller  
98 Schmied et al., 2014). [Only very limited studies attempt to calibrate global models on monthly discharge variations](#) (Werth

99 and Güntner, 2010). We desire efficient regionalized models that maximally leverage available information and provide  
100 accurate predictions to diverse basins across different climate groups and geographic characteristics in the world. We also want  
101 the models to perform decently even in data-sparse regions, showing competitive extrapolation ability, given that many large  
102 regions such as in Africa and Asia lack publicly available streamflow data. DL and differentiable models seem plausible  
103 candidates for such simulations. Nevertheless, previous studies on DL and physics-informed differentiable models mainly  
104 focus on continental or smaller scales, with a relatively homogeneous forcing dataset --- it is unclear if their observed strengths,  
105 e.g., high performance and strong generalization ability, can carry over to global scales, where the climate is much more diverse  
106 and datasets differ widely in their biases and uncertainty characteristics. In particular, we want to thoroughly examine how  
107 well these models can leverage information learned in data-rich continents to characterize the hydrologic processes in  
108 ungauged regions across the world. Meanwhile, DL models also show favorable scaling relationships (or data synergy) where  
109 more data leads to more robust models (Fang et al., 2022). Thus, training on a larger dataset may provide additional benefits.

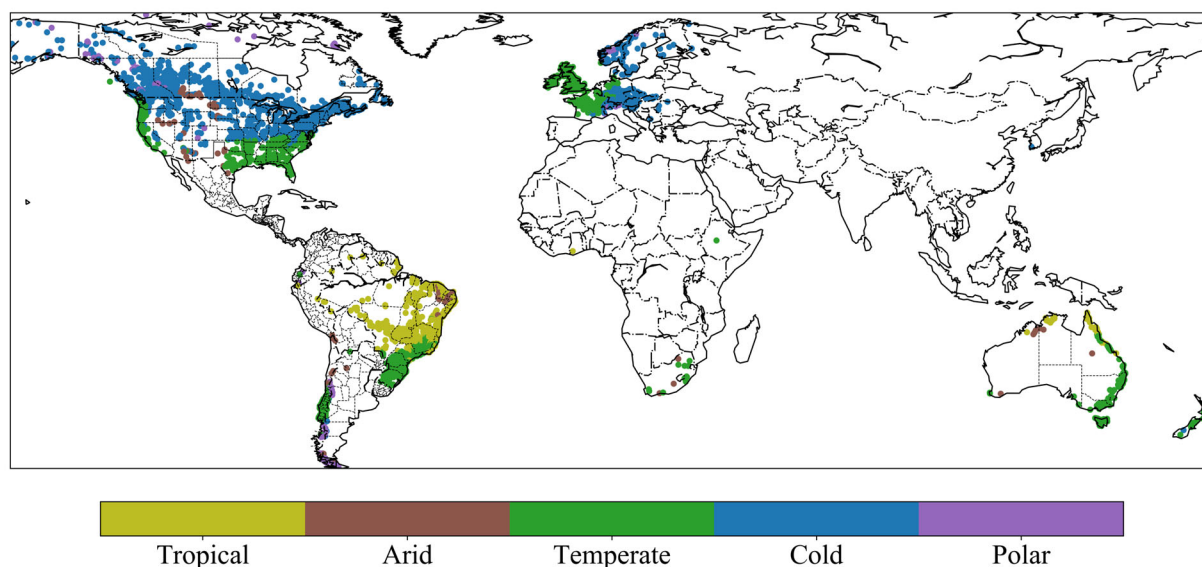
110  
111 In this study, we test physics-informed differentiable models (with the full version name  $\delta$ HBV-globe1.0-hydroDL, where “ $\delta$ ”  
112 represents “differentiable”, globe1.0 is the version, and “hydroDL” refers to our particular code implementation.  $\delta$ HBV is  
113 used as the abbreviation in this paper) to simulate hydrologic processes for global basins and compare results to purely data  
114 driven methods and traditional modeling approach. We focus on regionalized modeling and emphasize the importance of  
115 spatial generalization in data-sparse scenarios, since observed streamflow data in many parts of the world are scarce. This  
116 means one framework with parameter regionalization from geographic attributes will be used to model all the global basins  
117 rather than calibrating a separate model in each individual basin (Beck et al., 2020b; Feng et al., 2022; Mizukami et al., 2017).  
118 We first investigate what prediction accuracy can be achieved by different models at global scale by learning from a large and  
119 diverse dataset. We then relate the global spatial patterns of model performance to geographic characteristics and hydrologic  
120 processes to identify model structural deficiencies and gain hydrologic insights. Finally, we provide evidence indicating which  
121 type of model may be more appropriate for next-generation global modeling by rigorously examining their generalizability to  
122 ungauged regions across the world.

## 123 **2. Data and methods**

### 124 **2.1 Global datasets**

125 We use a global database compiled in a previous study (Beck et al., 2020b) which contains a total of 4229 headwater  
126 catchments. The dataset includes basin mean meteorological forcings, catchment characteristics such as the climate,  
127 topography, land cover, soil composition, and geology information to support parameter regionalization, along with streamflow  
128 gauge discharge observations. Meteorological forcings are the driving inputs of hydrological models. This global dataset  
129 includes daily precipitation from Multi-Source Weighted-Ensemble Precipitation (MSWEP), a product that merges gauge,  
130 satellite, and reanalysis precipitation data (Beck et al., 2017c, 2019), and maximum and minimum temperature from Multi-

131 Source Weather (MSWX), a product that bias-corrects and harmonizes meteorological data from atmospheric reanalyses and  
132 weather forecast models (Beck et al., 2022). Potential evapotranspiration was estimated using the method from Hargreaves  
133 (1994). The discharge observations at the outlet gauges were used as prediction targets to train the hydrologic models. We  
134 excluded some basins with potential erroneous discharge records such as showing unreasonable magnitude way larger than  
135 precipitation or dramatic differences between two time intervals, by manually performing visual screening, and also excluded  
136 those with severe amounts of missing data (less than 5 years' worth of data points in the study period from 2000 to 2016).  
137 Thus, 3753 basins were finally used to evaluate different models. These basins had been classified into five Köppen-Geiger#  
138 climate classes in Beck et al., (2020b), including tropical (489 basins), arid (109 basins), temperate (1423 basins), cold (1593  
139 basins), and polar (139 basins), as shown in Figure 1. To evaluate the simulations of untrained variables like evapotranspiration  
140 (ET), the MOD16A2GF (Running et al., 2021), a gap-filled 8-day composite ET product estimated from the Moderate  
141 Resolution Imaging Spectroradiometer (MODIS) satellite data and meteorological reanalysis data, were used as independent  
142 observations to compare against the simulated ET from differentiable hydrologic models.

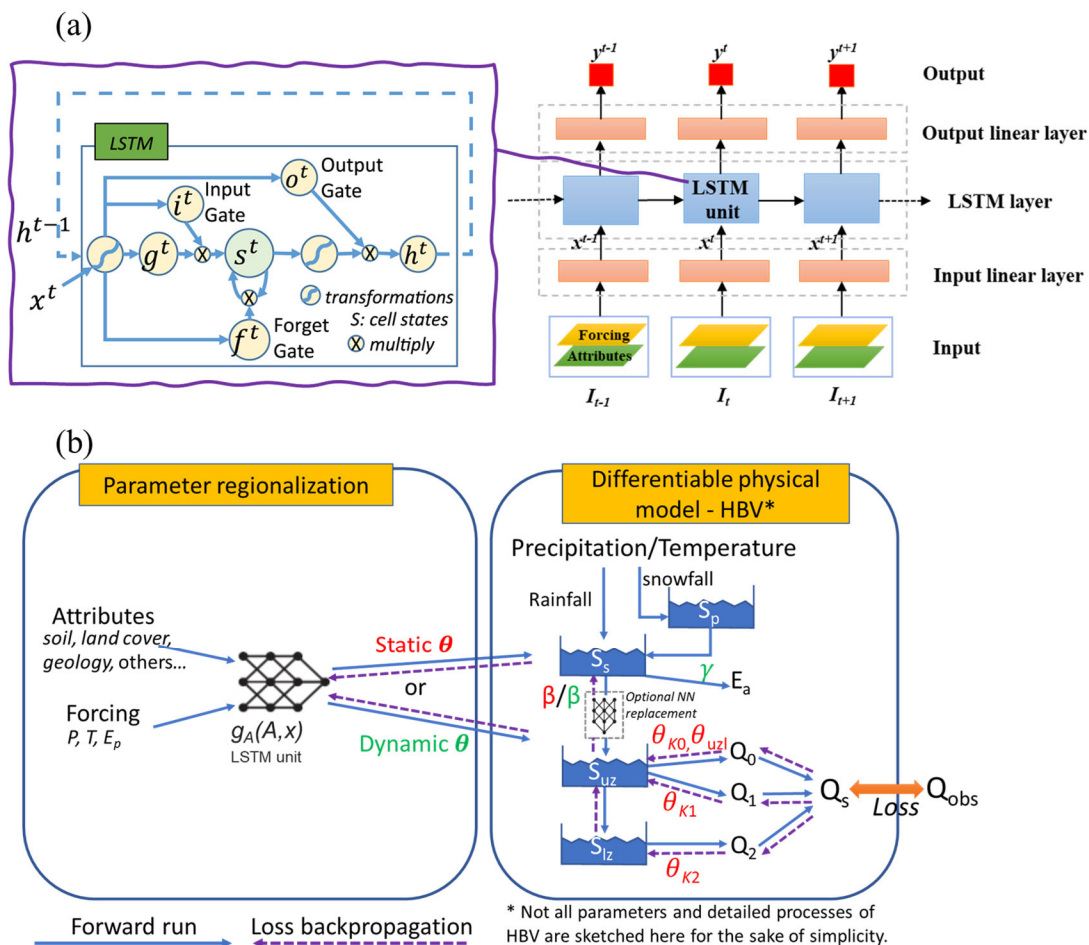


143  
144 *Figure 1. Locations and climate groups of the 3753 global basins used in this study, which were originally compiled by Beck et al., 2020.*  
145 *Plotted in Python using Matplotlib Basemap Toolkit.*

## 146 2.2 The long short-term memory (LSTM) streamflow model for comparison

147 Here the LSTM model is used as a benchmark for purely data-driven DL. The LSTM has “cell states” and “gates” to maintain  
148 and filter information, as shown in Figure 2a. The input, forget, and output gates control the flow of information, respectively  
149 controlling what to let in, what to forget, and what to output from the system. In this study we use the LSTM streamflow model  
150 demonstrated in Feng et al. (2020) which has been successfully applied to simulate streamflow in hundreds of basins across  
151 the CONUS. The framework takes meteorological forcings and basin attributes as inputs and generates daily streamflow

152 predictions for each basin at each time step (Figure 2a). We used mini-batches to train the LSTM model, where each minibatch  
 153 was composed of two-year sequences from 256 randomly-selected basins. The first-year sequences are only used for  
 154 initializing the cell states, so we calculate the batch loss function only on the second-year sequences. The training sequences  
 155 were also randomly selected from the whole training period, and one epoch was finished when the model had seen all the  
 156 training data. Note that this sequence length is a subset of, and different concept from, the length of training period. Sequence  
 157 length specifically refers to the length of the training instance that comprises a minibatch, whereas training period refers to the  
 158 whole period when observations are available for training, from which the minibatch sequence length is randomly selected.  
 159 The model was forwarded on each minibatch iteratively and its weights were updated using gradient descent after each  
 160 forwarding. One epoch was considered to have occurred when the model is iterated over all the training data. We trained the  
 161 LSTM model for 300 epochs to achieve convergence.



162

163 **Figure 2. Illustrations of two different types of regionalized hydrologic models. (a) Framework of the purely data-driven LSTM**  
 164 **streamflow model (adapted from Figure 2 in Feng et al., 2020), and (b) framework of the differentiable HBV model ( $\delta$ HBV-globe1.0-**  
 165 **hydroDL) with parameter regionalization developed in Feng et al. (2022) (adapted from Figure 1 in Feng et al. (2022)). The neural**



166 *network  $g_A$  here is a LSTM unit which is trained by the observed streamflow to produce the static or dynamic physical HBV parameters*  
167 *( $\theta, \beta, \gamma$ ) from basin characteristics.*

### 168 **2.3 The hybrid differentiable hydrologic models**

169 We used the hybrid differentiable models ( $\delta$ HBV-globe1.0-hydroDL) developed in Feng et al., (2022) for regionalized  
170 modeling in global basins. The HBV model used here as the physical backbone is a conceptual hydrologic model with  
171 representations of snowpack, soil, and groundwater storages, and can simulate flux variables such as snow melting,  
172 evapotranspiration, and quick and slow outflows (Beck et al., 2020b; Bergström, 1976, 1992; Seibert and Vis, 2012). The  
173 differentiable parameter learning (dPL) framework (Tsai et al., 2021) is used to provide parameter regionalization for HBV,  
174 as shown by the  $g_A$  neural network in Figure 2b. The  $g_A$  network, which is a LSTM unit here, takes basin attributes and  
175 meteorological forcings as inputs, and outputs static or dynamic physical HBV parameters. The differentiable HBV model  
176 then takes these parameters as well as the meteorological forcings to simulate the hydrological process and predict daily  
177 streamflow discharge along with other key flux variables. The whole framework including HBV itself was implemented in a  
178 DL platform (PyTorch 1.0.1 was used for the original development and the model has also shown good compatibility with  
179 more recent PyTorch versions, (Paszke et al., 2017)) supporting automatic differentiation and trained with gradient descent to  
180 minimize the difference between the simulated and observed streamflow (the loss function). As in Feng et al., (2022), we  
181 employed the loss function based on root-mean-square error (RMSE) with two weighted parts. The first part calculates RMSE  
182 directly on the simulated and observed discharge, while the second part calculates RMSE on the transformed discharge records  
183 to improve low flow representations. Note that we do not directly train the HBV parameters; rather, we focus on training the  
184 weights of the  $g_A$  neural network to map the relationship between basin-averaged characteristics and HBV parameters.  
185 [Differentiable models are also trained in mini-batches that are formed in the same way as for training the LSTM streamflow](#)  
186 [model. Within one epoch, differentiable models are forwarded and optimized over the randomly formed mini-batches until the](#)  
187 [iterations have used all the training data points. We train the differentiable models for 50 epochs in total.](#)

188  
189 As described in Feng et al. (2022), the differentiable modeling framework enables optional modification of the structures of  
190 the original HBV model to enable better performance and we use two versions of evolved HBV models in this study. We used  
191 16 parallel subbasin-scale response units, each with a separate set of parameters to describe a fraction of the basin with different  
192 hydrologic responses. These components implicitly represent subbasin-scale spatial heterogeneity. The simulated fluxes (e.g.,  
193 streamflow) are the average of all the response units. The parameters of the multiple components are different and all are  
194 produced simultaneously by the same  $g_A$  network. The first version of our model (referred to as “dPL + evolved HBV”) only  
195 has static parameters which are kept constant during the hydrologic simulation. The second version (referred to as “dPL +  
196 evolved HBV with DP) further allows some formerly static parameters of the multi-component model to vary daily with the  
197 meteorological forcings. These dynamic parameters (DP) were also produced by the  $g_A$  LSTM unit. If we were to apply the  
198 dynamic parameterization to all parameters, the model could become overly flexible, potentially leading to overfitting to the  
199 training data (which would lead to issues with extrapolation beyond the training data). To reduce the risk of overfitting, we

200 restricted the dynamism to only two empirical parameters: the shape coefficient  $\beta$  in the equation that describes the  
201 relationships between soil storage and potential runoff, and a newly added shape parameter ( $\gamma$ ) which is involved in the  
202 calculation of evapotranspiration. For more details regarding these differentiable HBV models, please refer to our previous  
203 studies (Feng et al., 2022, 2023).

## 204 2.4 Experiments and evaluation metrics

205 We ran one temporal and two spatial generalization experiments to evaluate the performance of different regionalized models.  
206 For the temporal generalization experiment, the models were trained for the period of 2000 to 2016 on all global basins, and  
207 tested for the period of 1980 to 1997. [Basins without discharge records or with less than 5 years' worth of data points in the](#)  
208 [testing period were excluded from the evaluation.](#) Without spatially holding out any basin during training, this experiment  
209 aimed at evaluating the model's generalizability in the time dimension by testing prediction ability on the same basins but in  
210 a different time period from the training data. The other two spatial generalization experiments served as the true litmus tests  
211 for evaluating the effectiveness of regionalization schemes, i.e., how well the model can be applied to basins that have never  
212 been seen during training. The first spatial generalization experiment was a traditional "prediction in ungauged basins" (PUB)  
213 problem, where we randomly divided the whole global basin set into 10 folds (groups) and performed cross-validation across  
214 these folds to obtain spatial out-of-sample predictions for all basins (training on 9 of the folds with the 10th fold held out and  
215 testing on the 10th, then rotating such that each fold is used for testing once). The second spatial generalization experiment,  
216 which we refer to as cross-continent "prediction in ungauged regions" (PUR), was more challenging. In this experiment, we  
217 assumed that all the basins in certain continents are ungauged and excluded from the training dataset, trained a regionalized  
218 model in other data-rich continents, and then tested the trained model to make predictions in the ungauged continents. With  
219 random hold-out, an ungauged test basin in the first spatial generalization experiment always has training gauges surrounding  
220 it. Therefore, the first PUB experiment can be interpreted as spatial interpolation. The second spatial experiment (cross-  
221 continent PUR) holds out all the basins in one continent as testing targets, and thus is the much harder test of spatial  
222 extrapolation.

223

224 To evaluate the overall performance of the hydrologic models, we used the Kling-Gupta Efficiency (KGE)<sub>2</sub> (Gupta et al., 2009;  
225 Kling et al., 2012) as compared in Beck et al., (2020b) and Nash-Sutcliffe Efficiency (NSE)<sub>2</sub> (Nash and Sutcliffe, 1970). KGE  
226 has three components that account for correlation, mean bias, and variability bias, while NSE mainly represents the variance  
227 explained by the simulations. Both metrics indicate better performance when their values are closer to the maximum value of  
228 1. We also examined the percent bias of the top 2% peak flow range (FHV) and bottom 30% low flow range (FLV) of  
229 streamflow predictions to evaluate the model's ability to simulate extreme events (Yilmaz et al., 2008). All the reported  
230 performance metrics in this study are from model evaluation on the testing dataset, which is not seen by the model during the  
231 training process.



## 232 3. Results and discussions

### 233 3.1 General patterns over global basins

234 From the standpoint of daily hydrograph metrics (KGE and NSE), LSTM and the two differentiable models all achieved highly  
235 competitive performance for the global basins in the temporal test (trained and tested on the same basins, but in different time  
236 periods) (Figure 3). For the global dataset, all three models obtained median KGE values close to or higher than 0.7, but the  
237 LSTM model performed the best of the three models here, achieving a median NSE (KGE) value of 0.70 (0.74) for all the  
238 evaluated basins. For a subset of 1675 basins with long-term records (at least 15 years' worth of streamflow data available in  
239 the training period and 5 years' worth of data available in the testing period, though not necessarily continuous), LSTM even  
240 reached a [median KGE of 0.78 \(see Figure A1\)](#). Both versions of the differentiable models approached the performance level  
241 of the LSTM, in agreement with our previous assessment for the CONUS (Feng et al., 2022). The model with dynamic  
242 parameters achieved a median NSE (KGE) of 0.67 (0.69), followed by the model with static parameters, which obtained a  
243 median NSE (KGE) of 0.65 (0.68).

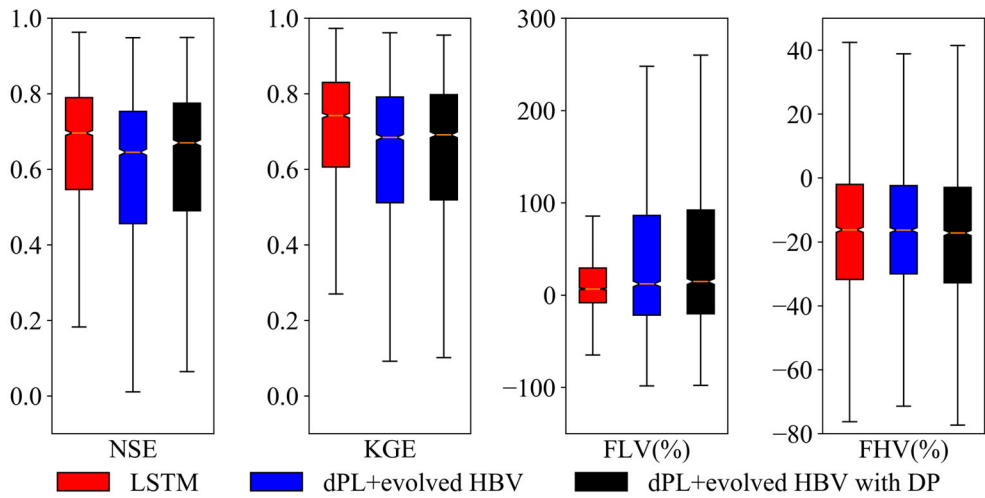
244

245 The LSTM exhibited advantages for the low flow predictions compared with the differentiable models, as shown by the FLV  
246 metric (Figure 3). However, for the peak flow predictions, the LSTM and differentiable models were quite similar, and they  
247 all underestimated the observed peaks (FHV in Figure 3). The underestimation for peak flows is consistent with what was  
248 found in previous studies. For example, all the physical and deep learning models have significant negative peak flow bias  
249 when benchmarked in the CONUS dataset (Feng et al., 2020; Kratzert et al., 2019b). We hypothesize that the systematic  
250 underestimation of peaks may be partially related to bias in precipitation forcings. MSWEP is based on the ERA5 reanalysis,  
251 which is known to underestimate precipitation peaks (Beck et al., 2019). Furthermore, the use of basin-averaged, daily-  
252 averaged precipitation may further suppress the peaks (Chen et al., 2017). In addition, the errors with peak flow could also be  
253 partly due to some numerical and structural issues with the differentiable models, e.g., numerical errors introduced by the  
254 explicit and sequential solution scheme of HBV with excessive use of threshold functions that lead to different results when  
255 the sequence changes, and structure limitations, e.g., deeper groundwater storage cannot feed back to the upper layers. Given  
256 the commonality of this issue, we call for community efforts and collaboration to address this issue.

257

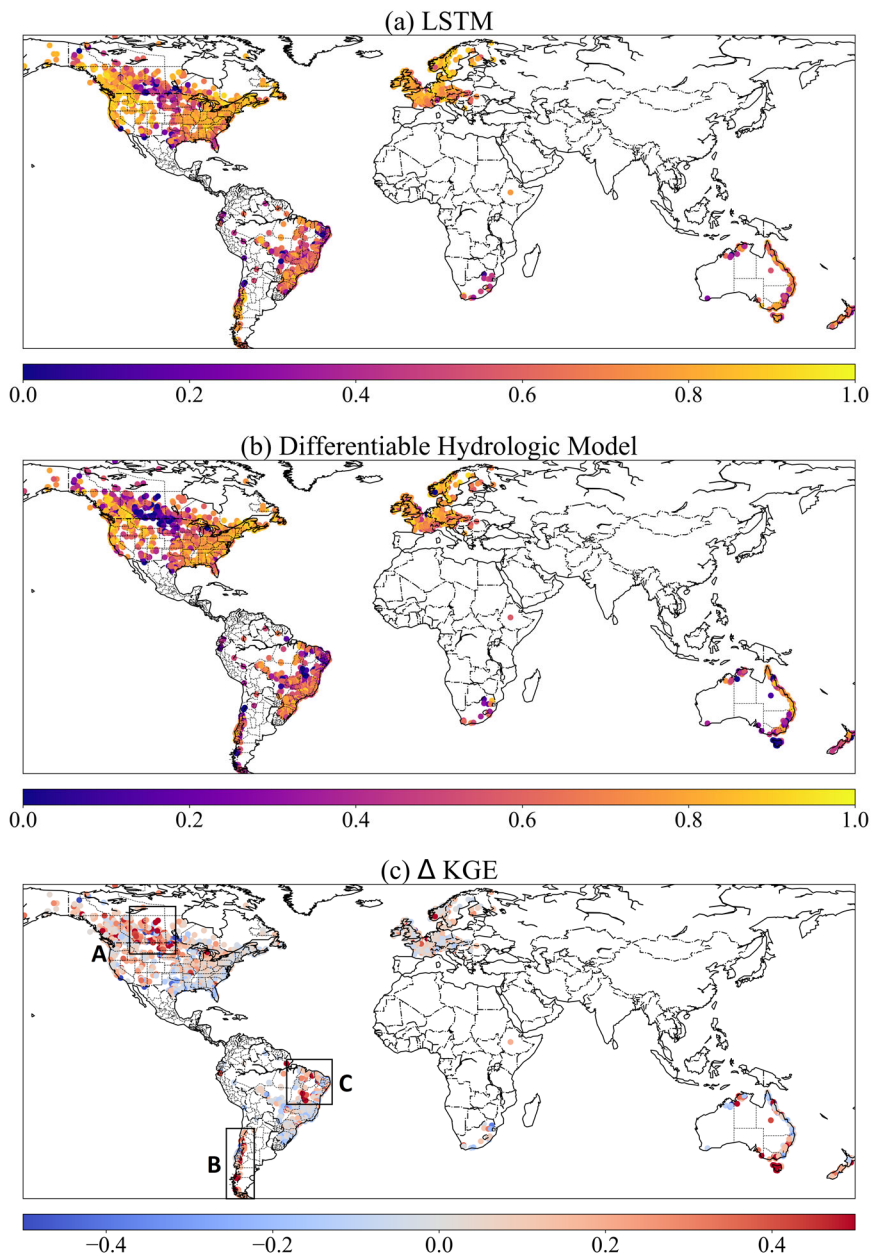
258 Both the LSTM model and the differentiable models performed well over diverse landscapes, including North America  
259 (especially along the Rocky and Appalachian mountain ranges and the Southeastern Coastal Plains), Western Europe, Asia  
260 (mostly Japan), the southern part of Brazil, and the northeast coast of Australia (Figure 4a and b). There are other regions  
261 where none of the three models performed well, such as the longitudinally-central part of North America (Great Plains and  
262 Interior Lowlands), the southern edge of Chile (with many glaciers), the Tasmania state of Australia, and the few basins in  
263 Africa. These regions, for example, the Northern Great Plains and the state of Texas in the CONUS, have always been difficult  
264 for all kinds of models, likely due to incorrect basin boundary, highly localized precipitation, the dry conditions with small

265 runoff amounts and flash flooding mechanisms (Berghuijs et al., 2014; Driscoll et al., 2002; Feng et al., 2020; Martinez and  
 266 Gupta, 2010; Newman et al., 2017), to be explored below. Despite some challenges, however, these values represent currently  
 267 the best metrics reported at the global scale compared to earlier studies, e.g., (Alfieri et al., 2020; Beck et al., 2017a, 2020b;  
 268 Hou et al., 2023), attesting to these models' great potential as global modeling tools.  
 269



270  
 271 **Figure 3. Performance comparison between the LSTM and differentiable models on global basins. dPL refers to the differentiable**  
 272 **parameter learning framework, while “evolved HBV” refers to some modifications to improve the standard HBV model, and “with DP”**  
 273 **indicates that some parameters were allowed to be dynamic rather than static. Here, the horizontal line inside the colored box represents**  
 274 **the median, while the top and bottom of the colored box indicate the first and third quartiles. The bars extending from the colored boxes**  
 275 **indicate 1.5 times the interquartile range from the first and third quartiles. NSE is Nash-Sutcliffe Efficiency, KGE is Kling-Gupta**  
 276 **Efficiency, FLV indicates the model’s percent bias on the bottom 30% low flow range of streamflow, and FHV indicates percent bias on**  
 277 **the top 2% peak flow range of streamflow.**

278



279

280 *Figure 4. The spatial patterns of different model performance and their differences shown by KGE metric. (a) the LSTM model; (b) the*  
 281 *differentiable model with dynamic parameters (dPL + evolved HBV with DP); and (c) the KGE difference between two models (KGE of*  
 282 *LSTM – KGE of dPL + evolved HBV with DP). Plotted in Python using Matplotlib Basemap Toolkit.*

### 283 3.2 Model behaviors and limitations across climate groups and regions

284 All three models' performances vary significantly across different climate groups of the global basins (Figure 5), revealing  
285 their strengths and limitations. The LSTM model behaved the best in the polar, cold, and temperate groups, while the  
286 performance deteriorated in the tropical and arid basins. Similar to LSTM, differentiable models showed strong performance  
287 in temperate and cold groups and worse performance in tropical ones, with the worst performance in arid basins. These clusters  
288 of challenging basins can also be identified on the map (Figure 4a and b). [The differentiable model with dynamic parameters](#)  
289 [performed better than the model with static parameters in all climate groups except the most challenging arid group. Dynamic](#)  
290 [parameterization with more structural flexibility generally provides stronger modeling ability, while also showing a higher risk](#)  
291 [of overfitting and degraded generalizability in basins which are very difficult to simulate.](#) As we examine how LSTM and  
292 differentiable models behave differently, we find that such differences can be attributed to processes missing from the simple  
293 backbone process-based model (HBV here) as explained below. Here we use LSTM as an indicator of upper bound, that is, it  
294 shows the ideal performance of a model, given the available information from forcing and input data. Thus the distance from  
295 LSTM indicates either systematic and predictable forcing errors (which can be remediated by LSTM) or structural issues with  
296 the differentiable model.

297

298 For example, the polar group stands out as a climate type favoring LSTM, while the cold group shows a similar but less  
299 pronounced contrast, both of which may be related to HBV's physical deficiencies and forcing issues with snow undercatch.  
300 For the polar (cold) groups, LSTM surprisingly had a median KGE of 0.81 (0.78) while the differentiable model only reached  
301 0.62 (0.71). The polar regions include, for example, Southern Chile (in region B in Figure 4c). As glaciers can store water for  
302 extended periods of time and are driven mostly by temperature rather than rainfall, it is possible for LSTM to capture the  
303 temperature-driven dynamics (Lees et al., 2022) while the original HBV itself does not have a glacial module. HBV does not  
304 have the ability to simulate frozen soil, sublimation or snow cover fractions. Furthermore, as snow gauges in high altitude are  
305 known to suffer systematic bias due to undercatch problems (Beck et al., 2020a), LSTM can learn to address such systematic  
306 bias while physical differentiable models cannot due to mass balance. For the cold regions, e.g., high-latitude regions of the  
307 North American Great Plains (Region A in Figure 4c --- this also includes the Prairie Pothole Region, or PPR), HBV may  
308 suffer from not having descriptions for frozen ground conditions (soil ice) which can influence infiltration, and rainfall  
309 underestimation due to undercatch, ice blockage, and other potential reasons (Beck et al., 2020a). In addition, another reason  
310 why LSTM and differentiable HBV may have trouble with PPR (but HBV performed especially poorly) is the countless  
311 wetlands that store water until full and become connected after snowmelt and large rainfall. HBV does not have modules that  
312 can describe such large-scale fill-connect-spill processes (Shaw et al., 2013; Vanderhoof et al., 2017).

313

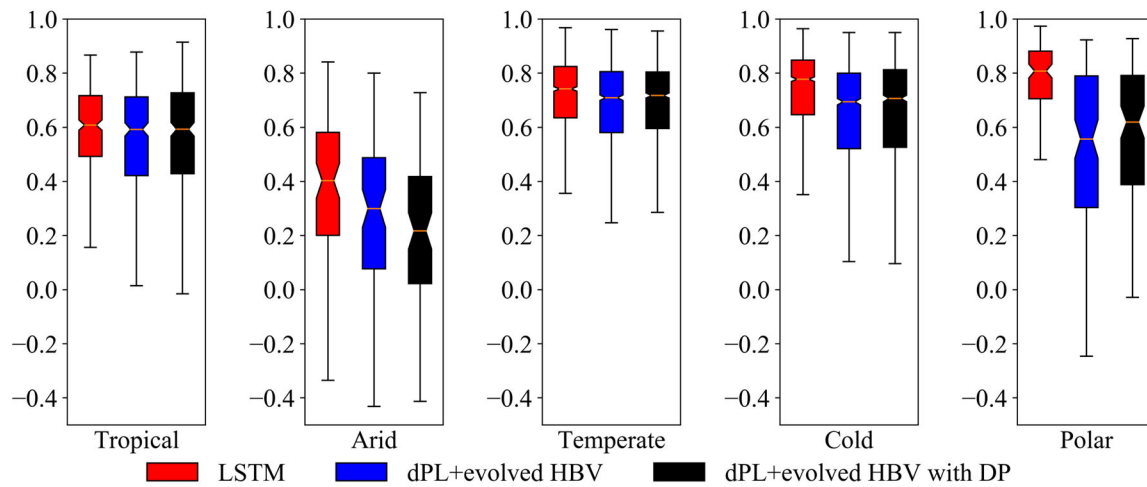
314 A more prominent challenge is the arid regions (middle CONUS, north Chile and east Brazil in Figure 1 and Figure 4). This  
315 challenge can be attributed to the long duration of low flows which requires long-term memory, and flash floods which result

316 from intense short-duration storms not well represented at the daily scale. Even the LSTM model cannot retain year-long  
 317 memory and cannot perform well for the baseflow (Feng et al., 2020). Because HBV has a linear reservoir for its slow-flow  
 318 (lowest) bucket, it cannot generate zero base flows. Neither can it well simulate the impact of intense hourly-scale rainfall.  
 319 These process improvements need to be considered in the future. Another reason for the challenge in arid regions is the lack  
 320 of reservoir management modules. Arid regions tend to have water management infrastructure that significantly influences  
 321 streamflow (Veldkamp et al., 2018). Since the HBV model doesn't have any module representing human impacts on the natural  
 322 water cycle, the poor performance in middle Brazil in region C may have come from the missing representation of human  
 323 interferences. There are large population and intensive agricultural activities in this region which could induce significant  
 324 impacts on the hydrologic process. Parameter compensations apparently cannot make up for all the missing mechanisms.

325

326 The sensitivity of model performance to missing processes in the differentiable models is both good and bad news. It's good  
 327 news because this means we can identify suitable or insufficient process representations by learning from data. On the other  
 328 hand, this means more challenges as we need to increase the process complexity of this model before it can perform well for  
 329 these basins, unlike the purely data-driven LSTM which is not explicitly concerned with physical processes.

330



331

332 *Figure 5. The performance comparison (KGE, Kling-Gupta Efficiency) of different models for five climate groups. dPL refers to the*  
 333 *overall differentiable parameter learning framework, while “evolved HBV” refers to some modifications to improve the standard HBV*  
 334 *model, and “with DP” indicates that some parameters were allowed to be dynamic rather than static. Here, the horizontal line inside the*  
 335 *colored box represents the median, while the top and bottom of the colored box indicate the first and third quartiles. The bars extending*  
 336 *from the colored boxes indicate 1.5 times the interquartile range from the first and third quartiles.*

### 337 3.3 Spatial generalization for prediction in ungauged regions

338 While LSTM maintains mild advantages over differentiable models in data-dense settings, it was outperformed by  
 339 differentiable models in a highly data-scarce scenario. As mentioned above, the data-dense setting was tested in the randomized

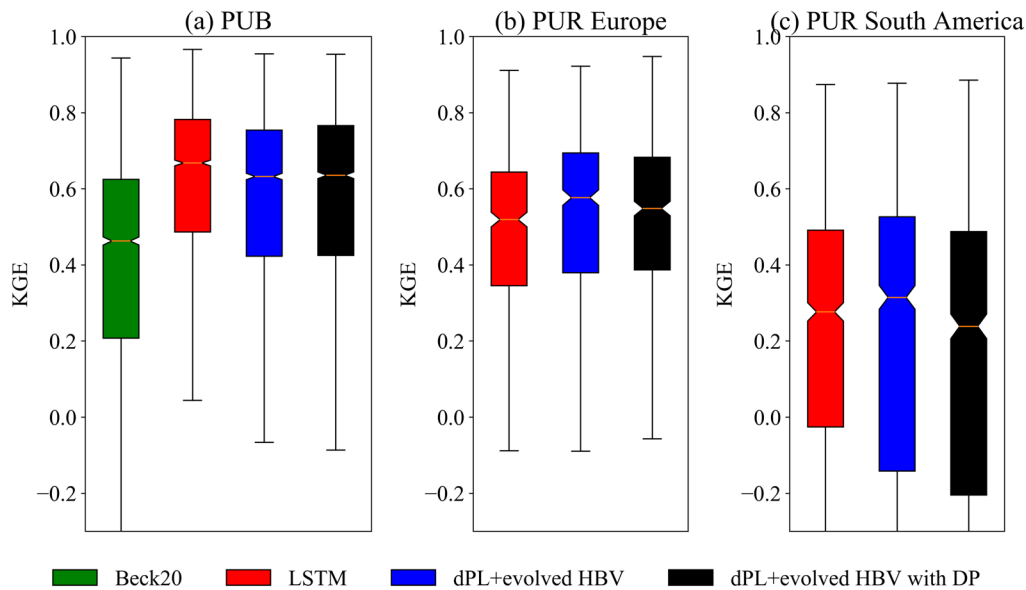
340 holdout test called prediction in ungauged basins (PUB), while the data-scarce scenario was tested in the regional holdout test,  
341 or prediction in ungauged regions (PUR). In the global PUB test, LSTM has a small edge (median KGE=0.67) over  
342 differentiable models (median KGE=0.64). Both were noticeably higher than the traditional regionalization method using  
343 linear transfer functions reported by Beck et al. (2020b) (Beck20, median KGE=0.46), which already represents the previous  
344 state-of-the-art performance of global parameter regionalization. Differentiable modeling does not rely on strong assumptions  
345 of the functional form for the parameter transfer function. It leverages the powerful ability of neural networks to represent  
346 complicated functions, and automatically learns robust and generalizable relationships between geographic attributes and  
347 physical model parameters from large data. Therefore, we can expect significant performance advantages from differentiable  
348 modeling compared to traditional methods relying on linear transfer functions. In the PUR scenario where European basins  
349 were held out for testing, differentiable models (median KGE=0.58) performed significantly better ([p-value less than 0.01](#)  
350 [using the one-sided Wilcoxon signed-rank test](#)) than LSTM (median KGE=0.52). In the South American PUR experiment,  
351 lower performance was seen for all models which can be expected considering the prediction difficulties in this region even  
352 for the in-sample scenario (Region B and C in Figure 4). The median KGE of LSTM is 0.28 while the differentiable model  
353 with static parameters achieves a higher median KGE of 0.31 for the PUR scenario. It seemed that the differentiable model  
354 with dynamic parameterization was somewhat overfitted in this case, resulting in a median KGE that was lower than the static-  
355 parameter differentiable model. We do not have PUR results from traditional models available to compare against, since this  
356 is a very challenging issue for traditional regionalization methods to make predictions across continents.

357

358 [With these results, we show that differentiable models have demonstrated a high simulation capability that cannot be obtained](#)  
359 [with traditional parameter regionalization approaches, and also provide a robust extrapolation capability in large data-sparse](#)  
360 [regions](#) that is stronger than purely data-driven models like LSTM. ~~[With these results, we show that differentiable models have](#)~~  
361 ~~[demonstrated a robust capability for spatial generalization that cannot be obtained by straightforwardly training models on](#)~~  
362 ~~[data alone.](#)~~ This conclusion was not only verified in the USA, but now has also been confirmed in [global catchments with](#)  
363 [generalization tests including prediction in neighboring ungauged basins and](#) cross-continent predictions ~~[in Europe and South](#)~~  
364 ~~[America](#)~~, each of which have ~~[different](#)~~[unique](#) conditions with respect to data [availability and](#) density.

365





366

367 *Figure 6. The performance comparison (KGE, Kling-Gupta Efficiency) of different models for spatial generalization tests. (a) Random*  
 368 *hold-out test for prediction in ungauged basins (PUB), (b) and (c) holding out all the basins in Europe or South America, respectively,*  
 369 *for cross-continent predictions in ungauged regions (PUR). Beck20 refers to a traditional regionalization method using linear transfer*  
 370 *functions (Beck et al., 2020b), LSTM is the purely data-driven long short-term memory network, dPL refers to the differentiable*  
 371 *parameter learning framework, while “evolved HBV” refers to some modifications to improve the standard HBV model, and “with DP”*  
 372 *indicates that some parameters were allowed to be dynamic rather than static. Here, the horizontal line inside the colored box represents*  
 373 *the median, while the top and bottom of the colored box indicate the first and third quartiles. The bars extending from the colored boxes*  
 374 *indicate 1.5 times the interquartile range from the first and third quartiles.*

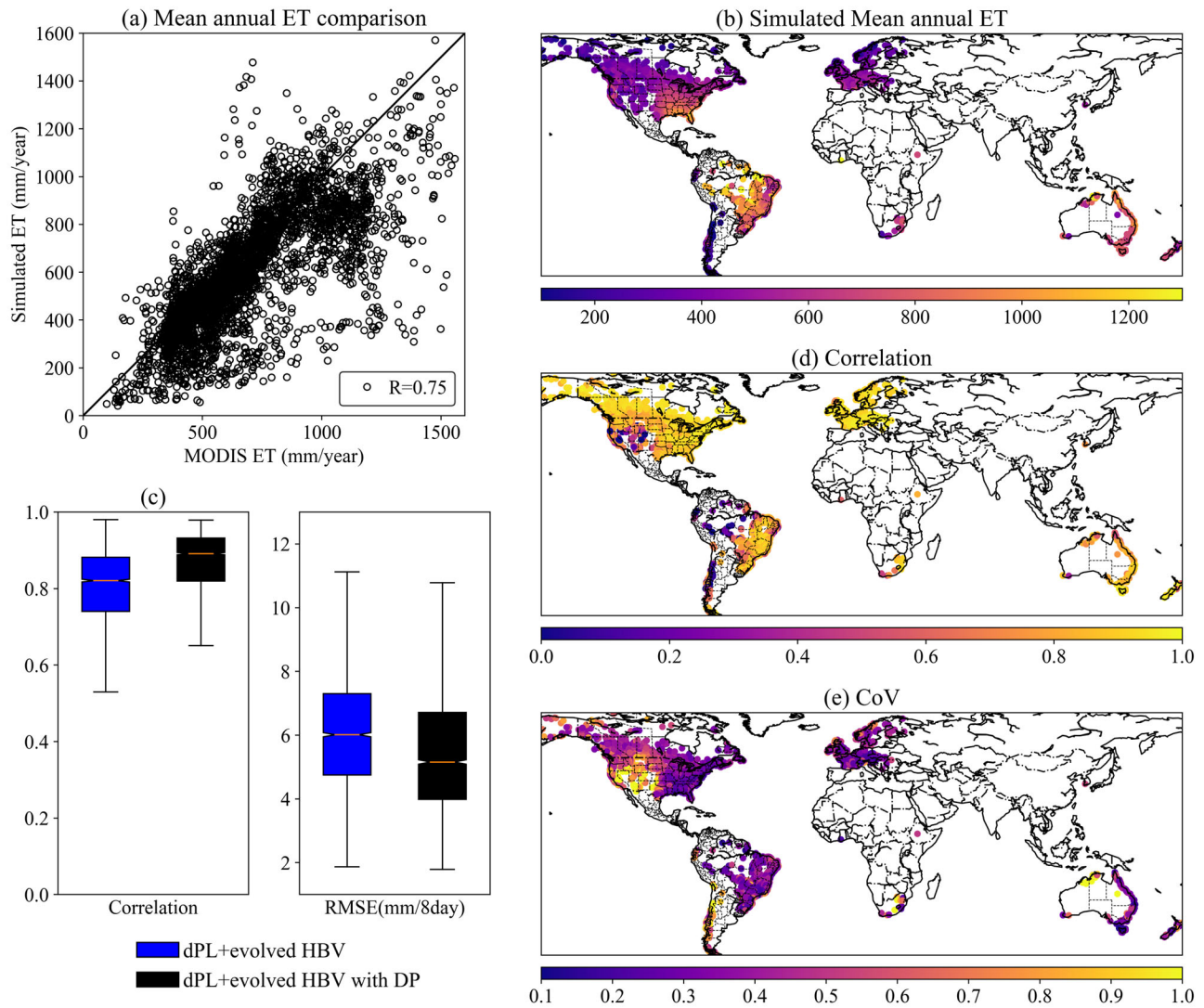
### 375 3.4 Predicting untrained variables

376 The evapotranspiration (ET) simulations from differentiable models are consistent with independent MODIS satellite estimates  
 377 of ET in both temporal dynamics and spatial patterns. We did not use any ET observations as training targets to supervise the  
 378 differentiable models. At the global scale, the mean annual ET comparison shows overall consistency with MODIS, with most  
 379 basins lying close to the 1:1 line and a correlation of 0.75 for all the basins (Figure 7a). Spatially, the model was able to  
 380 represent energy limitations in the cold regions, e.g., high-latitude North America and Europe, and water limitations, e.g.,  
 381 southwestern US and arid basins of Australia (Figure 7a and b). The model also represented high ET in basins adjacent to the  
 382 Amazon forest, those along the US southeastern and Australian coast. Temporally, the median correlation of ET time series  
 383 between simulations and MODIS products achieves 0.82 and 0.89 for two differentiable models in 3753 basins, respectively  
 384 (Figure 7c).

385

386 The ET simulations show high correlation with MODIS in most North American and European basins (Figure 7d), in line with  
 387 the good performance of streamflow modeling in these regions. However, the correlation is relatively lower in South America  
 388 but the coefficient of variation of ET residuals (CoV, the ratio of standard deviation of ET residuals to the annual mean) is also

389 small (Figure 7e), in part because the ET here is large and less driven by the seasonal energy cycle (Niu et al., 2017). MODIS  
390 ET itself is not the ground truth and always has large uncertainties in Amazonia regions due to the cloud coverage and  
391 difficulties for observation (Hilker et al., 2015; Xu et al., 2019). Furthermore, the simulations could be negatively influenced  
392 by the data quality issues with streamflow records in these regions. Upon examining the records, some stations in South  
393 America show unrealistic hydrographs that may indicate data processing errors. To address such issues in the future, more in-  
394 depth data screening and correction or constraining the model using datasets other than streamflow, e.g., eddy covariance flux  
395 data, should be considered. The CoV is less than 0.3 for most of the world, showing that ET errors are mostly small relative to  
396 its annual averages (Figure 7e). Noticeable exceptions are US southwest, where ET varies strongly from year to year and is  
397 highly dependent on the precipitation, and Chile, where glaciers and deserts are both present, posing challenges to the model.  
398 As the present study is basin-focused, we will leave the evaluation of global gridded ET to future work.  
399



400

401 *Figure 7. The comparison between simulated ET from the differentiable hydrologic models and independent MODIS ET product. (a)*  
 402 *mean annual ET comparison, (b) simulated mean annual ET for global basins, (c) boxplots for the temporal dynamic evaluation by*  
 403 *correlation and RMSE, (d) correlation and (e) coefficient of variation for ET comparison in global basins. Maps plotted in Python using*  
 404 *Matplotlib Basemap Toolkit.*

405 **3.5 Further discussion**

406 [Compared to the LSTM model which only outputs discharge simulations, differentiable models offer a suite of interpretable](#)  
 407 [variables including ET, soil water, recharge, baseflow, etc., thus providing a comprehensive description for the hydrologic](#)  
 408 [cycle and far better interpretability. To create a new differentiable model or turn an existing model into a differentiable one,](#)  
 409 [we need to implement the model on a differentiable platform like PyTorch, Tensorflow, or JAX, while better enabling model](#)  
 410 [parallelism in order to maximally leverage the computing power of modern graphical processing units \(GPUs\). If a model](#)

411 [contains mostly explicit calculations](#), automatic differentiation (AD) offered by the above platforms can effortlessly provide  
412 [gradient calculations](#), requiring only a syntax-level translation which can nowadays be done easily. Sometimes, a limited  
413 [amount of adjustments](#) are needed to turn non-differentiable operations into equivalent differentiable ones. However, when a  
414 [model contains iterative solutions to nonlinear systems](#), large matrix solvers or constrained optimizations, we can employ the  
415 [adjoint method](#) (Song et al., 2023). [The adjoint method explicitly defines the gradient-calculation method and alters the order](#)  
416 [of calculations so iteration is avoided during gradient calculations](#), which can dramatically reduce memory demand and  
417 [improve efficiency](#). Another important consideration is the effective use of [parallelism](#) and the modern computing  
418 [infrastructure for AI](#) (i.e., GPUs). In our context, the regionalized parameterization (in this case, training one neural network  
419 [on a large amount of basins](#)), which is crucial to ensuring the generalizability of the model, requires going through large data  
420 [in high-throughput parallelism](#). Embracing parallelism may necessitate some coding adjustments. At this point, several  
421 [versions of differentiable hydrologic models have been proposed with varying complexities and different handling of](#)  
422 [parameterization, post-processing](#) (which we didn't use in this study, as it can interfere with interpretability of the internal  
423 [variables, mass balances, and the sensitivity to inputs encoded by the process-based components](#)), and dynamical parameters.  
424 [Across geoscientific domains, differentiable ecosystem](#) (Aboelyazeed et al., 2023; Zhao et al., 2019), [streamflow and river](#)  
425 [routing](#) (Bindas et al., 2024), [water quality](#) (Rahmani et al., 2023), and [ice sheet](#) (Bolibar et al., 2023) [models have already](#)  
426 [been demonstrated](#). Some central differences exist between the differentiable modeling approach and the traditional calibration  
427 [approach](#): First, we always attempt to train differentiable models over a large collection of sites, improving the robustness and  
428 [efficiency of learning](#). Second, we reimplemented the model onto PyTorch in a parallel fashion, and were thus able to leverage  
429 [the high concurrency and computing power offered by modern GPUs](#). Third, the commonalities between sites and the  
430 [accumulation of knowledge in the neural network further improves the efficiency of training compared to traditional training](#)  
431 [done individually for each site, as the knowledge learned from one batch is inherited when the neural network is trained on the](#)  
432 [next batch](#). Fourth, differentiable models can flexibly evolve the structure of the physical backbone. The two types of  
433 [differentiable models used in this study have used multiple isparallel components per basin to represent subbasin-scale](#)  
434 [heterogeneity](#). For the models with dynamic parameterization, two parameter values vary at each daily time step as a function  
435 [of the meteorological forcings](#). It seems unrealistic to use traditional parameter calibration to optimize these models with  
436 [evolved structures](#). However, leveraging automatic differentiation and gradient descent, differentiable models can  
437 [automatically learn to produce large amounts of parameters from geographic attributes through the embedded neural networks](#).

438

439 The challenges facing [the differentiable models in this study](#) include not only missing processes like reservoir management,  
440 ground ice, and glaciers, but also large errors in [meteorological forcings](#) and streamflow target [data](#). Substantial bias could  
441 exist in precipitation, e.g., due to snow-gauge undercatch (Hou et al., 2023), or in discharge, e.g., streamflow are measured  
442 using different approaches which exhibit large variability; for another example, gridded climate forcing data often consistently  
443 underestimate the magnitudes of heavy storms (Beck et al., 2017b). While LSTM can easily adapt to systematic bias, such  
444 forcing errors put the differentiable models under stress because they cannot reconcile streamflow observations with such

445 forcings given the constraint of mass balances. If our objective is to learn core physics and parameterizations that are reliable  
446 despite forcing discrepancies, we can set up forcing data correction layers that can, to some extent, shield the core processes  
447 from being influenced by such errors. This will be an important aspect of future work to ensure reliable prediction of future  
448 water resources.

449

450 The backbone of a differentiable process-based model thus serves as a double-edged sword: when such backbones are  
451 essentially correct, they serve as a stabilizing element of the model that mitigates overfitting and improves generalization;  
452 when they lack critical processes or when observations have large, unexplained bias, they can drag down model performance  
453 and cause compensation between processes. However, the limitations are tractable: future work can gradually incorporate  
454 critical processes and include more observations to constrain the learning process, making sure each addition is valuable and  
455 accretive. The research community collectively has already substantial experience in evolving earth system models to include  
456 many processes. We expect some processes to be invited back in the differentiable modeling framework. Nevertheless, with  
457 differentiable modeling, we now have a new tool that was not previously available: highly flexible deep neural networks that  
458 can be placed anywhere in the model, which provide a systematic way of managing model complexity. With their help, such  
459 model evolution may take much less time than previously required. [However, we still expect the development cycle to take  
460 longer than for purely data-driven models like LSTM, requiring us to view differentiable models as evolving rather than static  
461 entities, which need a bit of patience while maturing.](#)

462

463 This study builds a benchmark and a basis for model selection and diagnosis for the next-generation global hydrologic  
464 modeling, which previously did not learn from such large observations. With rigorous tests at [the](#) global scale, this study proves  
465 that differentiable models are strong candidates as global water models. With powerful spatial generalization ability, they can  
466 be applied to characterizing the hydrologic processes in ungauged regions by leveraging learned information in data-rich  
467 continents. Differentiable models in this study have already learned the generalizable and robust relationships between  
468 geographic attributes and physical model parameters from thousands of global catchments. Therefore, these models can be  
469 easily applied towards providing seamless global hydrologic modeling with parameters directly generated from worldwide  
470 geographic attributes. Future work can use such models to produce global hydrologic fluxes while enhancing some process  
471 representations in extremely arid, glaciated, or heavily human-influenced basins.

#### 472 **4. Conclusions**

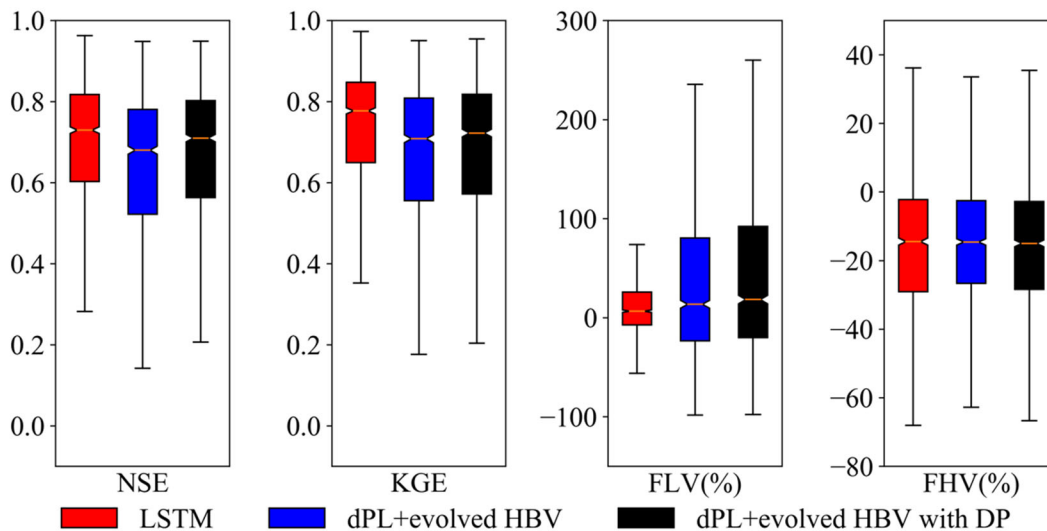
473 In this work, we used both purely data-driven models and, for the first time, physics-informed, differentiable models to simulate  
474 rainfall-runoff processes in 3753 global basins. Both types of models achieved overall highly competitive performance for  
475 global basins with diverse climate conditions, yielding median KGE values close to or higher than 0.7 which is state-of-the-  
476 art at this large scale. The LSTM still achieved the best performance for the temporal generalization test, but the differentiable

477 HBV models with evolved structure ( $\delta$ HBV-globe1.0-hydroDL) approach the LSTM's performance level. Furthermore, the  
478 spatial generalization experiments highlighted the stronger regionalization and extrapolation ability of differentiable models  
479 than LSTM, demonstrating its promise to be applied to data-scarce regions in the world. Routing is not included in this work  
480 and will be investigated in the future, possibly also with differentiable approaches (Bindas et al., 2022).

481

482 Different models appear to have generally consistent spatial performance patterns, though obvious distinctions stand out in  
483 several local regions. All models achieve good performance in the temperate and cold climate groups, while they all behave  
484 unsatisfactorily in the arid group. For the polar group, the differentiable model performed significantly worse than the LSTM.  
485 Without any physical constraints, LSTM shows strong power in simulating storage (snow and glacier) dominated processes,  
486 while differentiable models are limited by the structure of their physical backbone model, which in this case does not simulate  
487 multiyear ice buildup and melt. Another limitation could be soil sealing processes in extremely arid regions. These regional  
488 performance comparisons thus reveal some deficiencies of the physical backbone in  $\delta$ HBV that cannot be mitigated even by  
489 advanced neural network-based parameterization. These insights provide directions for future improvements. Different from  
490 purely data-driven models only trained by the target variable, differentiable models constrained by the physical backbone can  
491 give accurate simulations for a full set of hydrologic variables in the water cycle including evapotranspiration, snow water  
492 equivalent, water storage, infiltration and baseflow. As some process limitations are addressed in the future, we believe  
493 differentiable models will be strong candidates for the next generation global water models to characterize and predict the  
494 hydrologic processes in ungauged regions across the world.

## 495 Appendix



496



497 [Figure A1. Performance comparison on the 1675 subset basins with long-term streamflow records \(at least 15 years' worth](#)  
498 [of streamflow data available in the training period and 5 years' worth of data available in the testing period, not necessarily](#)  
499 [continuous\). Other items are the same as in Figure 3.](#)  
500

#### 501 **Author contributions**

502 DF and CS conceived this study. DF set up the hydrologic models and ran all the experiments. DF and CS performed the major  
503 analysis, with HB, JdB, RKS, YS, YW and MP contributing substantially to the discussions on the methodology and results.  
504 HB provided the global dataset and the benchmark results from a traditional regionalization scheme. JL prepared the ET  
505 product for comparison. DF wrote the initial draft and CS revised the manuscript. HB, JdB, RKS, YS, YW, and KL  
506 substantially edited the manuscript.

#### 507 **Financial support**

508 DF was supported by the National Science Foundation Award EAR-2221880. This work was also partially supported and  
509 inspired by the Young Scientists Summer Program (YSSP) of International Institute for Applied Systems Analysis (IIASA).  
510 JL was supported by Google.org's AI Impacts Challenge Grant 1904-57775. CS and KL were supported by Cooperative  
511 Institute for Research to Operations in Hydrology (CIROH), award number A22-0307-S003. Computation was partially  
512 supported by the National Science Foundation Major Research Instrumentation Award PHY-2018280.

#### 513 **Code and Data Availability**

514 The source codes for the differentiable hydrologic models can be accessed at <https://doi.org/10.5281/zenodo.7091334>, and this  
515 study evaluates these models at global scale. The MOD16A2GF ET product can be downloaded at  
516 <https://lpdaac.usgs.gov/products/mod16a2gfv061/>. Meteorological forcing datasets MSWEP and MSWX can be downloaded  
517 at <https://www.gloh2o.org/mswep/> and <https://www.gloh2o.org/mswx/>, respectively. The streamflow observations used in this  
518 study were initially compiled by Beck, Pan, et al., (2020b) and can be accessed from the original data sources including the  
519 United States Geological Survey (USGS) National Water Information System (NWIS; <https://waterdata.usgs.gov/nwis>), the  
520 Global Runoff Data Centre (GRDC; <https://grdc.bafg.de>), the HidroWeb portal of the Brazilian Agência Nacional de Águas  
521 (<https://www.snirh.gov.br/hidroweb>), the European Water Archive (EWA) of EURO-FRIEND-Water  
522 ([https://www.bafg.de/GRDC/EN/04\\_spcldtbss/42\\_EWA/ewa.html](https://www.bafg.de/GRDC/EN/04_spcldtbss/42_EWA/ewa.html)) and the CCM2-JRC CCM River and Catchment Database  
523 (<https://data.jrc.ec.europa.eu/collection/ccm>), Water Survey of Canada (WSC) National Water Data Archive (HYDAT;  
524 <https://wateroffice.ec.gc.ca/>), the Australian Bureau of Meteorology (BoM; <http://www.bom.gov.au/waterdata/>), and the  
525 Chilean Center for Climate and Resilience Research (CR2) website (<https://www.cr2.cl/datos-de-caudales/>).

526 **References**

- 527 Aboelyazeed, D., Xu, C., Hoffman, F. M., Liu, J., Jones, A. W., Rackauckas, C., Lawson, K., and Shen, C.: A differentiable,  
528 physics-informed ecosystem modeling and learning framework for large-scale inverse problems: demonstration with  
529 photosynthesis simulations, *Biogeosciences*, 20, 2671–2692, <https://doi.org/10.5194/bg-20-2671-2023>, 2023.
- 530 Alfieri, L., Lorini, V., Hirpa, F. A., Harrigan, S., Zsoter, E., Prudhomme, C., and Salamon, P.: A global streamflow reanalysis  
531 for 1980–2018, *Journal of Hydrology X*, 6, 100049, <https://doi.org/10.1016/j.hydroa.2019.100049>, 2020.
- 532 Beck, H. E., van Dijk, A. I. J. M., de Roo, A., Dutra, E., Fink, G., Orth, R., and Schellekens, J.: Global evaluation of runoff  
533 from 10 state-of-the-art hydrological models, *Hydrology and Earth System Sciences*, 21, 2881–2903,  
534 <https://doi.org/10.5194/hess-21-2881-2017>, 2017a.
- 535 Beck, H. E., Vergopolan, N., Pan, M., Levizzani, V., van Dijk, A. I. J. M., Weedon, G. P., Brocca, L., Pappenberger, F.,  
536 Huffman, G. J., and Wood, E. F.: Global-scale evaluation of 22 precipitation datasets using gauge observations and  
537 hydrological modeling, *Hydrology and Earth System Sciences*, 21, 6201–6217, <https://doi.org/10.5194/hess-21-6201-2017>,  
538 2017b.
- 539 Beck, H. E., van Dijk, A. I. J. M., Levizzani, V., Schellekens, J., Miralles, D. G., Martens, B., and de Roo, A.: MSWEP: 3-  
540 hourly 0.25° global gridded precipitation (1979–2015) by merging gauge, satellite, and reanalysis data, *Hydrology and Earth  
541 System Sciences*, 21, 589–615, <https://doi.org/10.5194/hess-21-589-2017>, 2017c.
- 542 Beck, H. E., Wood, E. F., Pan, M., Fisher, C. K., Miralles, D. G., Dijk, A. I. J. M. van, McVicar, T. R., and Adler, R. F.:  
543 MSWEP V2 Global 3-Hourly 0.1° Precipitation: Methodology and Quantitative Assessment, *Bulletin of the American  
544 Meteorological Society*, 100, 473–500, <https://doi.org/10.1175/BAMS-D-17-0138.1>, 2019.
- 545 Beck, H. E., Wood, E. F., McVicar, T. R., Zambrano-Bigiarini, M., Alvarez-Garreton, C., Baez-Villanueva, O. M., Sheffield,  
546 J., and Karger, D. N.: Bias correction of global high-resolution precipitation climatologies using streamflow observations from  
547 9372 catchments, *Journal of Climate*, 33, 1299–1315, <https://doi.org/10.1175/JCLI-D-19-0332.1>, 2020a.
- 548 Beck, H. E., Pan, M., Lin, P., Seibert, J., Dijk, A. I. J. M. van, and Wood, E. F.: Global fully distributed parameter  
549 regionalization based on observed streamflow from 4,229 headwater catchments, *Journal of Geophysical Research:  
550 Atmospheres*, 125, e2019JD031485, <https://doi.org/10.1029/2019JD031485>, 2020b.
- 551 Beck, H. E., van Dijk, A. I. J. M., Larraondo, P. R., McVicar, T. R., Pan, M., Dutra, E., and Miralles, D. G.: MSWX: Global  
552 3-hourly 0.1° bias-corrected meteorological data including near real-time updates and forecast ensembles, *Bulletin of the  
553 American Meteorological Society*, 103, E710–E732, <https://doi.org/10.1175/BAMS-D-21-0145.1>, 2022.
- 554 Berghuijs, W. R., Sivapalan, M., Woods, R. A., and Savenije, H. H. G.: Patterns of similarity of seasonal water balances: A  
555 window into streamflow variability over a range of time scales, *Water Resources Research*, 50, 5638–5661,  
556 <https://doi.org/10.1002/2014WR015692>, 2014.
- 557 Bergström, S.: Development and application of a conceptual runoff model for Scandinavian catchments, PhD Thesis, Swedish  
558 Meteorological and Hydrological Institute (SMHI), Norköping, Sweden, 1976.
- 559 Bergström, S.: The HBV model - its structure and applications, Swedish Meteorological and Hydrological Institute (SMHI),  
560 Norrköping, Sweden, 1992.

- 561 Bindas, T., Tsai, W.-P., Liu, J., Rahmani, F., Feng, D., Bian, Y., Lawson, K., and Shen, C.: Improving river routing using a  
562 differentiable Muskingum-Cunge model and physics-informed machine learning, *Water Resources Research*, 60,  
563 e2023WR035337, <https://doi.org/10.1029/2023WR035337>, 2024.
- 564 Bolibar, J., Sapienza, F., Maussion, F., Lguensat, R., Wouters, B., and Pérez, F.: Universal differential equations for glacier  
565 ice flow modelling, *Geoscientific Model Development*, 16, 6671–6687, <https://doi.org/10.5194/gmd-16-6671-2023>, 2023.
- 566 Burek, P., Satoh, Y., Kahil, T., Tang, T., Greve, P., Smilovic, M., Guillaumot, L., Zhao, F., and Wada, Y.: Development of  
567 the Community Water Model (CWatM v1.04) – a high-resolution hydrological model for global and regional assessment of  
568 integrated water resources management, *Geoscientific Model Development*, 13, 3267–3298, <https://doi.org/10.5194/gmd-13-3267-2020>, 2020.
- 570 [Chaemchuen, P., Song, Y., Rahmani, F., Zhi, W., Li, L., Liu, X., Boyer, E., Bindas, T., Lawson, K., and Shen, C.: Deep  
571 learning insights into suspended sediment concentrations across the conterminous United States: Strengths and limitations,  
572 <https://papers.ssrn.com/abstract=4322321>, 11 January 2023.](https://papers.ssrn.com/abstract=4322321)
- 573 Chen, B., Krajewski, W. F., Liu, F., Fang, W., and Xu, Z.: Estimating instantaneous peak flow from mean daily flow,  
574 *Hydrology Research*, 48, 1474–1488, <https://doi.org/10.2166/nh.2017.200>, 2017.
- 575 [Cui, G., Anderson, M., and Bales, R.: Mapping of snow water equivalent by a deep-learning model assimilating snow  
576 observations, \*J. Hydrol.\*, 616, 128835, <https://doi.org/10.1016/j.jhydrol.2022.128835>, 2023.](https://doi.org/10.1016/j.jhydrol.2022.128835)
- 577 Driscoll, D. G., Carter, J. M., Williamson, J. E., and Putnam, L. D.: *Hydrology of the Black Hills Area*, South Dakota, 2002.
- 578 Fang, K. and Shen, C.: Near-real-time forecast of satellite-based soil moisture using long short-term memory with an adaptive  
579 data integration kernel, *J. Hydrometeor.*, 21, 399–413, <https://doi.org/10.1175/jhm-d-19-0169.1>, 2020.
- 580 Fang, K., Shen, C., Kifer, D., and Yang, X.: Prolongation of SMAP to spatiotemporally seamless coverage of continental U.S.  
581 using a deep learning neural network, *Geophys. Res. Lett.*, 44, 11,030–11,039, <https://doi.org/10.1002/2017gl075619>, 2017.
- 582 Fang, K., Pan, M., and Shen, C.: The value of SMAP for long-term soil moisture estimation with the help of deep learning,  
583 *IEEE Trans. Geosci. Remote Sensing*, 57, 2221–2233, <https://doi.org/10.1109/TGRS.2018.2872131>, 2019.
- 584 Fang, K., Kifer, D., Lawson, K., Feng, D., and Shen, C.: The data synergy effects of time-series deep learning models in  
585 hydrology, *Water Resources Research*, 58, e2021WR029583, <https://doi.org/10.1029/2021WR029583>, 2022.
- 586 Feng, D., Fang, K., and Shen, C.: Enhancing streamflow forecast and extracting insights using long-short term memory  
587 networks with data integration at continental scales, *Water Resources Research*, 56, e2019WR026793,  
588 <https://doi.org/10.1029/2019WR026793>, 2020.
- 589 Feng, D., Lawson, K., and Shen, C.: Mitigating prediction error of deep learning streamflow models in large data-sparse  
590 regions with ensemble modeling and soft data, *Geophysical Research Letters*, 48, e2021GL092999,  
591 <https://doi.org/10.1029/2021GL092999>, 2021.
- 592 Feng, D., Liu, J., Lawson, K., and Shen, C.: Differentiable, learnable, regionalized process-based models with multiphysical  
593 outputs can approach state-of-the-art hydrologic prediction accuracy, *Water Resources Research*, 58, e2022WR032404,  
594 <https://doi.org/10.1029/2022WR032404>, 2022.

- 595 Feng, D., Beck, H., Lawson, K., and Shen, C.: The suitability of differentiable, physics-informed machine learning hydrologic  
596 models for ungauged regions and climate change impact assessment, *Hydrology and Earth System Sciences*, 27, 2357–2373,  
597 <https://doi.org/10.5194/hess-27-2357-2023>, 2023.
- 598 Gupta, H. V., Kling, H., Yilmaz, K. K., and Martinez, G. F.: Decomposition of the mean squared error and NSE performance  
599 criteria: Implications for improving hydrological modelling, *Journal of Hydrology*, 377, 80–91,  
600 <https://doi.org/10.1016/j.jhydrol.2009.08.003>, 2009.
- 601 Hagemann, S., Chen, C., Clark, D. B., Folwell, S., Gosling, S. N., Haddeland, I., Hanasaki, N., Heinke, J., Ludwig, F., Voss,  
602 F., and Wiltshire, A. J.: Climate change impact on available water resources obtained using multiple global climate and  
603 hydrology models, *Earth System Dynamics*, 4, 129–144, <https://doi.org/10.5194/esd-4-129-2013>, 2013.
- 604 Hansen, L. D., Stokholm-Bjerregaard, M., and Durdevic, P.: Modeling phosphorous dynamics in a wastewater treatment  
605 process using Bayesian optimized LSTM, *Computers & Chemical Engineering*, 160, 107738,  
606 <https://doi.org/10.1016/j.compchemeng.2022.107738>, 2022.
- 607 Hargreaves, G. H.: Defining and using reference evapotranspiration, *Journal of Irrigation and Drainage Engineering*, 120,  
608 1132–1139, [https://doi.org/10.1061/\(ASCE\)0733-9437\(1994\)120:6\(1132\)](https://doi.org/10.1061/(ASCE)0733-9437(1994)120:6(1132)), 1994.
- 609 Hattermann, F. F., Krysanova, V., Gosling, S. N., Dankers, R., Daggupati, P., Donnelly, C., Flörke, M., Huang, S., Motovilov,  
610 Y., Buda, S., Yang, T., Müller, C., Leng, G., Tang, Q., Portmann, F. T., Hagemann, S., Gerten, D., Wada, Y., Masaki, Y.,  
611 Alemayehu, T., Satoh, Y., and Samaniego, L.: Cross-scale intercomparison of climate change impacts simulated by regional  
612 and global hydrological models in eleven large river basins, *Climatic Change*, 141, 561–576, [https://doi.org/10.1007/s10584-](https://doi.org/10.1007/s10584-016-1829-4)  
613 016-1829-4, 2017.
- 614 Hilker, T., Lyapustin, A. I., Hall, F. G., Myneni, R., Knyazikhin, Y., Wang, Y., Tucker, C. J., and Sellers, P. J.: On the  
615 measurability of change in Amazon vegetation from MODIS, *Remote Sensing of Environment*, 166, 233–242,  
616 <https://doi.org/10.1016/j.rse.2015.05.020>, 2015.
- 617 Hochreiter, S. and Schmidhuber, J.: Long Short-Term Memory, *Neural Computation*, 9, 1735–1780,  
618 <https://doi.org/10.1162/neco.1997.9.8.1735>, 1997.
- 619 Höge, M., Scheidegger, A., Baity-Jesi, M., Albert, C., and Fenicia, F.: Improving hydrologic models for predictions and  
620 process understanding using neural ODEs, *Hydrology and Earth System Sciences*, 26, 5085–5102,  
621 <https://doi.org/10.5194/hess-26-5085-2022>, 2022.
- 622 Hou, Y., Guo, H., Yang, Y., and Liu, W.: Global Evaluation of Runoff Simulation From Climate, Hydrological and Land  
623 Surface Models, *Water Resources Research*, 59, e2021WR031817, <https://doi.org/10.1029/2021WR031817>, 2023.
- 624 Jayakrishnan, R., Srinivasan, R., Santhi, C., and Arnold, J. G.: Advances in the application of the SWAT model for water  
625 resources management, *Hydrological Processes*, 19, 749–762, <https://doi.org/10.1002/hyp.5624>, 2005.
- 626 Jiang, S., Zheng, Y., and Solomatine, D.: Improving AI system awareness of geoscience knowledge: Symbiotic integration of  
627 physical approaches and deep learning, *Geophysical Research Letters*, 47, e2020GL088229,  
628 <https://doi.org/10.1029/2020GL088229>, 2020.
- 629 Kling, H., Fuchs, M., and Paulin, M.: Runoff conditions in the upper Danube basin under an ensemble of climate change  
630 scenarios, *Journal of Hydrology*, 424–425, 264–277, <https://doi.org/10.1016/j.jhydrol.2012.01.011>, 2012.

- 631 Konapala, G., Kao, S.-C., Painter, S. L., and Lu, D.: Machine learning assisted hybrid models can improve streamflow  
632 simulation in diverse catchments across the conterminous US, *Environ. Res. Lett.*, 15, 104022, <https://doi.org/10.1088/1748-9326/aba927>, 2020.
- 634 Kraft, B., Jung, M., Körner, M., Koirala, S., and Reichstein, M.: Towards hybrid modeling of the global hydrological cycle,  
635 *Hydrology and Earth System Sciences*, 26, 1579–1614, <https://doi.org/10.5194/hess-26-1579-2022>, 2022.
- 636 Kratzert, F., Klotz, D., Herrnegger, M., Sampson, A. K., Hochreiter, S., and Nearing, G. S.: Toward improved predictions in  
637 ungauged basins: Exploiting the power of machine learning, *Water Resources Research*, 55, 11344–11354,  
638 <https://doi.org/10/gg4ck8>, 2019a.
- 639 Kratzert, F., Klotz, D., Shalev, G., Klambauer, G., Hochreiter, S., and Nearing, G.: Towards learning universal, regional, and  
640 local hydrological behaviors via machine learning applied to large-sample datasets, *Hydrology and Earth System Sciences*,  
641 23, 5089–5110, <https://doi.org/10.5194/hess-23-5089-2019>, 2019b.
- 642 Lees, T., Buechel, M., Anderson, B., Slater, L., Reece, S., Coxon, G., and Dadson, S. J.: Benchmarking data-driven rainfall–  
643 runoff models in Great Britain: a comparison of long short-term memory (LSTM)-based models with four lumped conceptual  
644 models, *Hydrology and Earth System Sciences*, 25, 5517–5534, <https://doi.org/10.5194/hess-25-5517-2021>, 2021.
- 645 Lees, T., Reece, S., Kratzert, F., Klotz, D., Gauch, M., De Bruijn, J., Kumar Sahu, R., Greve, P., Slater, L., and Dadson, S. J.:  
646 Hydrological concept formation inside long short-term memory (LSTM) networks, *Hydrology and Earth System Sciences*, 26,  
647 3079–3101, <https://doi.org/10.5194/hess-26-3079-2022>, 2022.
- 648 [Liu, J., Bian, Y., Lawson, K., and Shen, C.: Probing the limit of hydrologic predictability with the Transformer network, \*J. Hydrol.\*, 637, 131389, <https://doi.org/10.1016/j.jhydrol.2024.131389>, 2024.](https://doi.org/10.1016/j.jhydrol.2024.131389)  
649
- 650 Mai, J., Shen, H., Tolson, B. A., Gaborit, É., Arsenault, R., Craig, J. R., Fortin, V., Fry, L. M., Gauch, M., Klotz, D., Kratzert,  
651 F., O’Brien, N., Princz, D. G., Rasiya Koya, S., Roy, T., Seglenieks, F., Shrestha, N. K., Temgoua, A. G. T., Vionnet, V., and  
652 Waddell, J. W.: The Great Lakes Runoff Intercomparison Project Phase 4: the Great Lakes (GRIP-GL), *Hydrology and Earth  
653 System Sciences*, 26, 3537–3572, <https://doi.org/10.5194/hess-26-3537-2022>, 2022.
- 654 Maidment, D. R.: Conceptual Framework for the National Flood Interoperability Experiment, *JAWRA Journal of the  
655 American Water Resources Association*, 53, 245–257, <https://doi.org/10/f97pz3>, 2017.
- 656 Martinez, G. F. and Gupta, H. V.: Toward improved identification of hydrological models: A diagnostic evaluation of the  
657 “abcd” monthly water balance model for the conterminous United States, *Water Resources Research*, 46,  
658 <https://doi.org/10.1029/2009WR008294>, 2010.
- 659 Mizukami, N., Clark, M. P., Newman, A. J., Wood, A. W., Gutmann, E. D., Nijssen, B., Rakovec, O., and Samaniego, L.:  
660 Towards seamless large-domain parameter estimation for hydrologic models, *Water Resources Research*, 53, 8020–8040,  
661 <https://doi.org/10/gcg2dm>, 2017.
- 662 Müller Schmied, H., Eisner, S., Franz, D., Wattenbach, M., Portmann, F. T., Flörke, M., and Döll, P.: Sensitivity of simulated  
663 global-scale freshwater fluxes and storages to input data, hydrological model structure, human water use and calibration,  
664 *Hydrology and Earth System Sciences*, 18, 3511–3538, <https://doi.org/10.5194/hess-18-3511-2014>, 2014.
- 665 Nash, J. E. and Sutcliffe, J. V.: River flow forecasting through conceptual models part I — A discussion of principles, *Journal  
666 of Hydrology*, 10, 282–290, [https://doi.org/10.1016/0022-1694\(70\)90255-6](https://doi.org/10.1016/0022-1694(70)90255-6), 1970.

- 667 Newman, A. J., Mizukami, N., Clark, M. P., Wood, A. W., Nijssen, B., Nearing, G., Newman, A. J., Mizukami, N., Clark, M.  
668 P., Wood, A. W., Nijssen, B., and Nearing, G.: Benchmarking of a Physically Based Hydrologic Model, *Journal of*  
669 *Hydrometeorology*, 18, 2215–2225, <https://doi.org/10/gbwr9s>, 2017.
- 670 Niu, J., Shen, C., Chambers, J., Melack, J. M., and Riley, W. J.: Interannual variation in hydrologic budgets in an Amazonian  
671 watershed with a coupled subsurface - land surface process model, *Journal of Hydrometeorology*, 18, 2597–2617,  
672 <https://doi.org/10.1175/JHM-D-17-0108.1>, 2017.
- 673 Paszke, A., Gross, S., Chintala, S., Chanan, G., Yang, E., DeVito, Z., Lin, Z., Desmaison, A., Antiga, L., and Lerer, A.:  
674 Automatic differentiation in PyTorch, in: 31st Conference on Neural Information Processing Systems (NIPS 2017), Long  
675 Beach, CA, 2017.
- 676 Rahmani, F., Lawson, K., Ouyang, W., Appling, A., Oliver, S., and Shen, C.: Exploring the exceptional performance of a deep  
677 learning stream temperature model and the value of streamflow data, *Environ. Res. Lett.*, 16, 024025,  
678 <https://doi.org/10.1088/1748-9326/abd501>, 2021.
- 679 Rahmani, F., Appling, A., Feng, D., Lawson, K., and Shen, C.: Identifying structural priors in a hybrid differentiable model  
680 for stream water temperature modeling, *Water Resources Research*, 59, e2023WR034420,  
681 <https://doi.org/10.1029/2023WR034420>, 2023.
- 682 [Reichert, P., Ma, K., Höge, M., Fenicia, F., Baity-Jesi, M., Feng, D., and Shen, C.: Metamorphic testing of machine learning](https://doi.org/10.5194/hess-28-2505-2024)  
683 [and conceptual hydrologic models, \*Hydrol. Earth Syst. Sci.\*, 28, 2505–2529, <https://doi.org/10.5194/hess-28-2505-2024>, 2024.](https://doi.org/10.5194/hess-28-2505-2024)
- 684 Running, S., Mu, Q., Zhao, M., and Moreno, A.: MODIS/Terra Net Evapotranspiration Gap-Filled 8-Day L4 Global 500m  
685 SIN Grid V061, <https://doi.org/10.5067/MODIS/MOD16A2GF.061>, 2021.
- 686 Saha, G., Rahmani, F., Shen, C., Li, L., and Cibin, R.: A deep learning-based novel approach to generate continuous daily  
687 stream nitrate concentration for nitrate data-sparse watersheds, *Science of The Total Environment*, 878, 162930,  
688 <https://doi.org/10.1016/j.scitotenv.2023.162930>, 2023.
- 689 Seibert, J. and Vis, M. J. P.: Teaching hydrological modeling with a user-friendly catchment-runoff-model software package,  
690 *Hydrology and Earth System Sciences*, 16, 3315–3325, <https://doi.org/10/f22r5x>, 2012.
- 691 Shaw, D. A., Pietroniro, A., and Martz, L. w.: Topographic analysis for the prairie pothole region of Western Canada,  
692 *Hydrological Processes*, 27, 3105–3114, <https://doi.org/10.1002/hyp.9409>, 2013.
- 693 Shen, C.: A transdisciplinary review of deep learning research and its relevance for water resources scientists, *Water Resources*  
694 *Research*, 54, 8558–8593, <https://doi.org/10.1029/2018wr022643>, 2018.
- 695 Shen, C., Appling, A. P., Gentine, P., Bandai, T., Gupta, H., Tartakovsky, A., Baity-Jesi, M., Fenicia, F., Kifer, D., Li, L., Liu,  
696 X., Ren, W., Zheng, Y., Harman, C. J., Clark, M., Farthing, M., Feng, D., Kumar, P., Aboelyazeed, D., Rahmani, F., Song, Y.,  
697 Beck, H. E., Bindas, T., Dwivedi, D., Fang, K., Höge, M., Rackauckas, C., Mohanty, B., Roy, T., Xu, C., and Lawson, K.:  
698 Differentiable modelling to unify machine learning and physical models for geosciences, *Nat Rev Earth Environ*, 4, 552–567,  
699 <https://doi.org/10.1038/s43017-023-00450-9>, 2023.
- 700 Song, Y., Knoben, W. J. M., Clark, M. P., Feng, D., Lawson, K. E., and Shen, C.: When ancient numerical demons meet  
701 physics-informed machine learning: adjoint-based gradients for implicit differentiable modeling, *Hydrology and Earth System*  
702 *Sciences Discussions*, 1–35, <https://doi.org/10.5194/hess-2023-258>, 2023.



- 703 [Song, Y., Tsai, W.-P., Gluck, J., Rhoades, A., Zarzycki, C., McCrary, R., Lawson, K., and Shen, C.: LSTM-based data](#)  
704 [integration to improve snow water equivalent prediction and diagnose error sources, \*J. Hydrometeorol.\*, 25, 223–237,](#)  
705 <https://doi.org/10.1175/JHM-D-22-0220.1>, 2024.
- 706 Tsai, W.-P., Feng, D., Pan, M., Beck, H., Lawson, K., Yang, Y., Liu, J., and Shen, C.: From calibration to parameter learning:  
707 Harnessing the scaling effects of big data in geoscientific modeling, *Nat Commun*, 12, 5988, [https://doi.org/10.1038/s41467-](https://doi.org/10.1038/s41467-021-26107-z)  
708 [021-26107-z](https://doi.org/10.1038/s41467-021-26107-z), 2021.
- 709 Vanderhoof, M. K., Christensen, J. R., and Alexander, L. C.: Patterns and drivers for wetland connections in the Prairie Pothole  
710 Region, United States, *Wetlands Ecol Manage*, 25, 275–297, <https://doi.org/10.1007/s11273-016-9516-9>, 2017.
- 711 Veldkamp, T. I. E., Zhao, F., Ward, P. J., Moel, H. de, Aerts, J. C. J. H., Schmied, H. M., Portmann, F. T., Masaki, Y., Pokhrel,  
712 Y., Liu, X., Satoh, Y., Gerten, D., Gosling, S. N., Zaherpour, J., and Wada, Y.: Human impact parameterizations in global  
713 hydrological models improve estimates of monthly discharges and hydrological extremes: a multi-model validation study,  
714 *Environ. Res. Lett.*, 13, 055008, <https://doi.org/10.1088/1748-9326/aab96f>, 2018.
- 715 Werth, S. and Güntner, A.: Calibration analysis for water storage variability of the global hydrological model WGHM,  
716 *Hydrology and Earth System Sciences*, 14, 59–78, <https://doi.org/10.5194/hess-14-59-2010>, 2010.
- 717 Wunsch, A., Liesch, T., and Broda, S.: Groundwater level forecasting with artificial neural networks: a comparison of long  
718 short-term memory (LSTM), convolutional neural networks (CNNs), and non-linear autoregressive networks with exogenous  
719 input (NARX), *Hydrology and Earth System Sciences*, 25, 1671–1687, <https://doi.org/10.5194/hess-25-1671-2021>, 2021.
- 720 Xu, D., Agee, E., Wang, J., and Ivanov, V. Y.: Estimation of Evapotranspiration of Amazon Rainforest Using the Maximum  
721 Entropy Production Method, *Geophysical Research Letters*, 46, 1402–1412, <https://doi.org/10.1029/2018GL080907>, 2019.
- 722 Yilmaz, K. K., Gupta, H. V., and Wagener, T.: A process-based diagnostic approach to model evaluation: Application to the  
723 NWS distributed hydrologic model, *Water Resources Research*, 44, <https://doi.org/10.1029/2008WR007188>, 2008.
- 724 Zaherpour, J., Gosling, S. N., Mount, N., Schmied, H. M., Veldkamp, T. I. E., Dankers, R., Eisner, S., Gerten, D.,  
725 Gudmundsson, L., Haddeland, I., Hanasaki, N., Kim, H., Leng, G., Liu, J., Masaki, Y., Oki, T., Pokhrel, Y., Satoh, Y., Schewe,  
726 J., and Wada, Y.: Worldwide evaluation of mean and extreme runoff from six global-scale hydrological models that account  
727 for human impacts, *Environ. Res. Lett.*, 13, 065015, <https://doi.org/10.1088/1748-9326/aac547>, 2018.
- 728 Zhao, W. L., Gentine, P., Reichstein, M., Zhang, Y., Zhou, S., Wen, Y., Lin, C., Li, X., and Qiu, G. Y.: Physics-constrained  
729 machine learning of evapotranspiration, *Geophysical Research Letters*, 46, 14496–14507,  
730 <https://doi.org/10.1029/2019gl085291>, 2019.
- 731 Zhi, W., Feng, D., Tsai, W.-P., Sterle, G., Harpold, A., Shen, C., and Li, L.: From hydrometeorology to river water quality:  
732 Can a deep learning model predict dissolved oxygen at the continental scale?, *Environ. Sci. Technol.*, 55, 2357–2368,  
733 <https://doi.org/10.1021/acs.est.0c06783>, 2021.

734